A Low-Complexity ECG Feature Extraction Algorithm for Mobile Healthcare Applications

Evangelos B. Mazomenos, Dwaipayan Biswas, Amit Acharyya, Taihai Chen, Koushik Maharatna, *Member, IEEE*, James Rosengarten, John Morgan, and Nick Curzen

***Abstract*—This paper introduces a low-complexity algorithm for the extraction of the fiducial points from the electrocardiogram (ECG). The application area we consider is that of remote cardiovascular monitoring, where continuous sensing and processing takes place in low-power, computationally constrained devices, thus the power consumption and complexity of the processing algorithms should remain at a minimum level. Under this context, we choose to employ the discrete wavelet transform (DWT) with the Haar function being the mother wavelet, as our principal analysis method. From the modulus-maxima analysis on the DWT coefficients, an approximation of the ECG fiducial points is extracted. These initial findings are complimented with a refinement stage, based on the time-domain morphological properties of the ECG, which alleviates the decreased temporal resolution of the DWT. The resulting algorithm is a hybrid scheme of time- and frequency-domain signal processing. Feature extraction results from 27 ECG signals from QTDB were tested against manual annotations and used to compare our approach against the state-of-the art ECG delineators. In addition, 450 signals from the 15-lead PTBDB are used to evaluate the obtained performance against the CSE tolerance limits. Our findings indicate that all but one CSE limits are satisfied. This level of performance combined with a complexity analysis, where the upper bound of the proposed algorithm, in terms of arithmetic operations, is calculated as $2.423N + 214$ additions and $1.093N + 12$ multiplications for $N \leq 861$ or $2.553N + 102$ additions and $1.093N + 10$ multiplications for $N > 861$ (N being the number of input samples), reveals that the proposed method achieves an ideal tradeoff between computational complexity and performance, a key requirement in remote cardiovascular disease monitoring systems.**

***Index Terms*—Discrete wavelet transform (DWT), electrocardiogram (ECG) feature extraction, low complexity algorithm, mobile healthcare.**

Manuscript received May 25, 2012; revised November 10, 2012; accepted November 21, 2012. Date of publication January 25, 2013; date of current version March 8, 2013. This work was supported by the European Union ARTEMIS joint undertaking under the Cyclic and person-centric Health management: Integrated appRoach for home, mobile and clinical eNvironments—(CHIRON) Project under Grant Agreement # 2009-1-100228.

E. B. Mazomenos, D. Biswas, T. Chen and K. Maharatna are with the School of Electronics and Computer Science, University of Southampton, Southampton, SO17 1BJ, U.K. (e-mail: ebm@ecs.soton.ac.uk; db9g10@ecs.soton.ac.uk; tc10g09@ecs.soton.ac.uk; km3@ecs.soton.ac.uk).

A. Acharyya is with the Department of Electrical Engineering, Indian Institute of Technology Hyderabad, Andhra Pradesh 502205, India (e-mail: amit_acharyya@iith.ac.in).

J. Rosengarten, J. Morgan, and N. Curzen are with the Southampton University Hospitals NHS Trust, Southampton, Hampshire, SO16 6YD, U.K. and also with the University of Southampton, Southampton, SO17 1BJ, U.K. (e-mail: james@rosengarten.co.uk; jmm@hrclinic.org; nick.curzen@suht.swest.nhs.uk).

Color versions of one or more of the figures in this paper are available online at http://ieeexplore.ieee.org.

Digital Object Identifier 10.1109/TITB.2012.2231312

I. Introduction

AGING population and continuous prevalence of cardiovascular diseases (CVD)—the number one cause of death (30% of the global total of all deaths) according to the World Health Organization (WHO)—leading to long-term conditions, have put current healthcare systems worldwide under serious strain in terms of the quality of care delivery and its associated cost [1]. Coupled with the ensuing productivity loss, this leads to a formidable socioeconomic challenge. Effective disease management through continuous monitoring and information fusion of vital physiological signals in chronic CVD patients is viewed as the key mechanism for the drastic reduction of the cost of CVD care delivery, the enhancement of the quality of care/life and the significant decrease in deaths and hospitalizations. Recently, advances in wireless sensor network (WSN) technology enabled the development of the next-generation remote CVD monitoring and management systems, able to monitor the patients' vital sign data continuously in nomadic environment. The main approach is to use a number of battery-powered wireless sensors to capture the vital signs and transmit all data to a centralized service for further analysis and disease prognosis. Since the traditional clinical feature extraction algorithms and information fusion techniques are, from a computational perspective, very intensive tasks, these parts are typically executed in main-frame type computational facilities. However, a significant energy expenditure component in such systems is the energy required by the radio front-end for supporting continuous data transmission, which may not allow a long-term sustainable operation. Taking as an example, the ECG signal—the fundamental component of a remote CVD monitoring system—captured at 1-kHz sampling rate with 16-bit quantization. Considering a typical Bluetooth V2 transceiver with 40–55 mA current consumption in transmission mode and a battery capacity of 1200 mAh (the typical batteries used for WSN applications) and following the analysis presented in [2], we conclude that continuous data transmission can be supported only for 24 h. In addition to this, A/D conversion, quantization, and signal preprocessing steps are also carried out at the sensor node and including those factors, it can be argued that the operation of a continuous transmission-based system, may not be realistically sustainable for more than 8–12 h. This falls well below the actual clinical notion of continuous monitoring in the sense of clinical usefulness.

The alternative approach for alleviating this problem—the approach adopted in the ARTEMIS Joint Undertaking funded CHIRON project of which this study is a part—is to carry out the feature extraction and information fusion operations, used to attain clinical diagnosis that are supposed to be carried out at

the main frame, at the sensor node itself and transmit the clinically relevant decisions to the centralized facility only upon request [3]. In this approach, the clinical results are stored on the sensor node itself and transmission takes place in burst mode at preset intervals or on-demand, therefore eliminating the requirement for continuous transmission while maintaining the notion of continuous monitoring. However, it may be argued that since the signal processing tasks required for such an approach are computationally intensive, the energy requirements for processing could overwhelm the energy required for continuous transmission. A recent attempt to implement an automated ECG delineation algorithm in a WSN node [4] indicated that the energy required for the ECG delineation is still significantly lower compared to the continuous transmission scenario, although it is pointed out that the selection of an appropriate algorithm, in terms of computational complexity and the type of microcontroller on which these operations will be executed, is of paramount importance in such a scenario.

Inspired by this fact, in this paper, we propose a novel automated ECG feature extraction algorithm that is specifically designed to be efficient from a computational perspective, thus ideal for ultralow-energy implementation. It is our belief that the proposed solution is suitable for integration in the latest generation remote CVD monitoring systems. It is important to point out that from a clinical application perspective, the main purpose of the automated ECG analysis in such remote monitoring systems is to produce an "alarm signal" if some abnormality is detected over a long period of time and by no means perform any detailed diagnosis of the patient's clinical condition, as this is eventually done through more elaborate diagnostic means (e.g., imaging techniques) in clinical settings. This fact prompts us to tradeoff accuracy and energy consumption although we show that the proposed system satisfies the CSE Working Party recommended tolerance limits [5] or is very close to them, when tested on standard databases, available in Physionet [6]. In addition, we have tested the proposed method on 12 conventional paper ECG signals supplied by the Southampton General Hospital Cardiology Department and the achieved accuracy in all cases is endorsed by expert cardiologists. The overall system consumes a mere 269 nW when synthesized in ST130 nm technology with 1.08-V supply voltage which clearly demonstrates its potential for low-power implementation.

The rest of this paper is structured as follows: after reviewing existing works in Section II, we describe our algorithm in Section III and provide an analysis of its computational complexity in Section IV. Section V is devoted for the validation of the algorithm, whereas conclusions are drawn in Section VI.

II. Background and Motivation

Traditionally, automated ECG analysis either takes place online on high-performance bedside devices which are bulky, or is done offline on ambulatory recordings provided by an ECG data logger, like the Holter device. The main task here is to automatically detect clinically important ECG fiducial points like the onset and offset of the QRS complex, P and T waves. These are then used to calculate various ECG parameters like the RR-interval, the QRS-length, the PR-interval, and the elevation/depression of the ST-segment. A plethora of excellent algorithms have been developed for such purpose based on different signal processing approaches, like the time-domain morphology (TDM) analysis augmented by different types of filtering [7]–[13], artificial neural networks [14], pattern matching [15], hidden Markov models [16], independent component analysis (ICA) [17] and combinations of the aforementioned methods [18]–[23]. Another significant line of approach is based on the wavelet transform (WT) which represents a signal in time-scale domain. Since the ECG signal is characterized by a periodic occurrence of patterns with different frequency contents, WT is deemed to be an excellent tool for its analysis. Subsequently, WT has been used extensively in the past [24]–[32]. In majority, WT-based ECG analysis algorithms use the quadratic spline wavelet as the basis function and employ the modulus-maxima analysis (MMA) method for finding out the peaks of characteristic waves at different resolution scales [33].

All the aforementioned algorithms show excellent performance in identifying the ECG fiducial points. However, the major concern associated with these algorithms is that they are extremely computationally intensive. As long as the operation is performed online on bulky bed-side devices or offline on a PC, their effectiveness is undoubted. But owing to the resource constrained nature—in particular, their limited battery life—of wearable wireless platforms these approaches may not be applicable, as the energy consumption is highly dependent on the computational complexity of the algorithmic process. Recently the WT-based ECG delineation algorithm proposed in [34] has been implemented on a commercially available Shimmer embedded sensor node which consists of an MSP430 microcontroller [35], showing that increased CPU activity leads to shorter node life-time. That work concludes that a careful study is necessary when choosing or designing a microcontroller [4]. However, the fundamental aspect of high computational complexity of the employed algorithms and the very fact that any general-purpose processor consumes several orders of magnitude more energy than an equivalent ASIC lead us to believe that the sensor node should be augmented with an ASIC, dedicated for the ECG analysis which needs to be designed following a holistic algorithm-architecture optimization approach. Therefore, in this study we concentrated on developing a low-complexity algorithm, ideal to be realized as a standalone ASIC, by exploiting the advantages of both WT and TDM analysis, which is described in the following sections.

III. Algorithmic Formulation

The main engineering requirement for our purpose is to develop a low-complexity algorithm for the automated ECG analysis leading to low-power consumption. On the other hand, the clinical requirement is that the algorithm needs to produce results of acceptable clinical quality. These two seemingly contradictory criteria put major constraints on the selection of the signal processing tools that can be employed, in the backdrop of their physical implementability for reducing the energy consumption. However, the very fact that the ECG in such systems

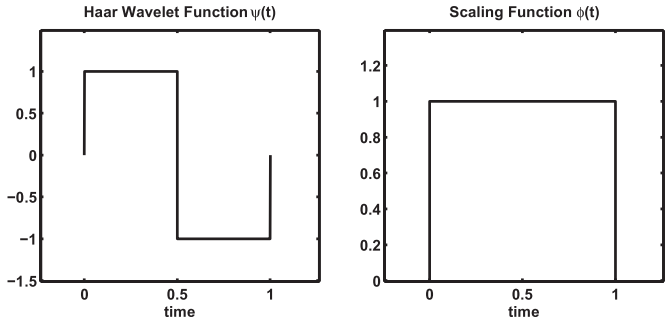

Fig. 1. Haar wavelet and scaling functions.

is mainly intended for generating an alarm allows one to tradeoff algorithmic accuracy, while still staying within the clinically acceptable levels, for energy consumption. In the following sections, we will present the step-by-step formulation of a novel algorithm satisfying this criterion.

A. Choice of the Wavelet function

Owing to the effectiveness of WT, we base our algorithm on this approach. The biggest advantage of WT is that because of its time-scale analysis nature, it is inherently able to separate noise and artifacts, like isoelectric line wandering, at its different resolution levels as already been shown in [34]. However, the mother wavelet used for this purpose is a computationally demanding quadratic-spline Wavelet and as mentioned previously has an impact on the energy consumption.

To keep the computational complexity low, we have selected the Haar wavelet—the simplest wavelet function. Although this function has its own limitations, we hypothesized that it still may be sufficient for the present purpose. The Haar wavelet function and its corresponding scaling function are depicted in Fig. 1.

To ascertain the effectiveness of the Haar DWT in dealing with noise and isoelectric line wandering, 450 ECG signals sampled at 1 kHz were investigated from the PTB database (PTBDB) [6]. Representative examples of signals that demonstrate isoelectric line wandering and signals that contain a significant amount of noise are illustrated alongside the five decomposition scales of Haar DWT in Fig. 2. It is obvious that significant noise components exist in the first two resolution levels. Therefore, applying MMA on these scales could lead to less accurate results. From our observations, we concluded that by employing the MMA on the 2^3 scale detailed DWT coefficients (cD_l3), an initial estimation of the QRS fiducial points, within the PQRST-complex, is possible. This is justified from Fig. 2 where in the 2^3 scale, noise components are suppressed to such a degree allowing for a noise-free representation of the ECG signal from the 2^3 scale onward. Therefore, for identifying the ECG waves, it is sufficient only to consider the 2^3 (for QRS) and 2^5 (for P/T waves) resolution scales. This implicitly means substantial reduction in the computational complexity. Nevertheless, operating exclusively on the 2^3 scale introduces the disadvantage of diminished temporal resolution due to downsampling. This is expected to add inaccuracies in the estimation of the QRS parameters. In addition, depending on the noise power and the statistical properties of the ECG signal, valid ECG frequency components may lie on the other resolution scales as well. Since we opt to operate on a single resolution scale these components will be discarded introducing further errors. Against this, our strategy is to refine the findings of the 2^3 scale MMA, by introducing a computationally efficient TDM-based compensatory step. This approach that we follow is ultimately justified by the obtained performance results (see Section V).

In a similar fashion, for the extraction of the P and T-waves parameters, instead of looking in multiple resolution levels, we focus entirely on the 2^5 scale. The reason for choosing the 2^5 scale is that the effect of the isoelectric line wandering in the 2^5 scale is minimal, as Fig. 2(a) illustrates and the P and T components are amplified in the 2^5 scale, compared to the 2^4 scale, enabling for a robust approximation of the P and T boundaries, considering that the QRS boundaries are already obtained. Fig. 2(c) depicts an extreme case where both noise and isoelectric line wandering are present in the ECG sample. Again, in the 2^3 and 2^5 scales of DWT decomposition, the prominent coefficients represent valid QRS-complexes and P and T waves which can be captured with the use of MMA. The reason for choosing a higher scale for the P and T waves is due to the fact that these waves comprise of lower frequency components than the QRS complex. The frequency response of the Haar DWT in the 2^3 and 2^5 scale is depicted in Fig. 3.

Contrary to our approach, other WT-based approaches conducted MMA on multiple-resolution levels. This multiple level MMA coupled with the use of computationally intensive mother wavelets can yield very accurate results for ECG delineation [27], [34]. However, we will demonstrate in our analysis (see Section IV) that the computational complexity, in terms of the arithmetic operations required, by the state of the art WT-delineator [34], which sets the basis of DWT-based ECG feature extraction, far exceeds the computational complexity of the proposed algorithm, even after including the TDM step. This, in combination with the obtained performance (see Section V) in a diverse set of ECG signals prompt us to conclude that the selection of the Haar function as the mother wavelet and the choice of operating exclusively on one DWT resolution scale, augmented by the TDM refinement step, enable the proposed algorithm to achieve the desired tradeoff of computational complexity and accuracy.

B. DWT-Based Initial Estimation

The proposed feature extraction method operates on a single isolated heartbeat (PQRST-complex) and initially assumes the presence of all the constituent ECG waves (P, QRS, and T). Our method is a combination of the MMA applied on the DWT decomposition levels and the time-domain morphological analysis of the ECG signal. Since we employ both frequency and time domain analysis, we refer to the resulting algorithm as the hybrid feature extraction algorithm (HFEA). To begin with, DWT decomposition takes place on the PQRST-complex. The analysis is performed at five dyadic space scales ($2^1 \cdots 2^5$) using the 2^3 and 2^5 scale for the extraction of QRS and P/T waves parameters,

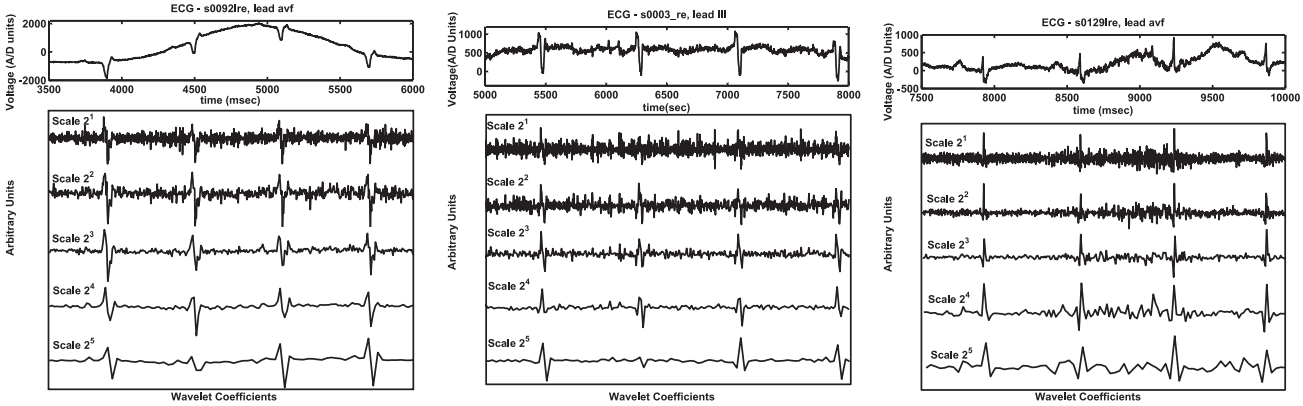

Fig. 2. ECG samples that (a) demonstrate isoelectric line wandering, (b) are corrupted with noise, (c) both, and their Haar DWT decomposition in five dyadic scales.

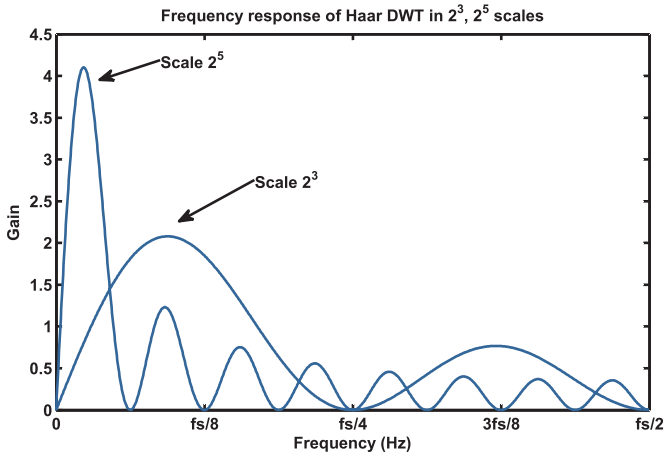

Fig. 3. Frequency response of the Haar DWT in scales 2^3 and 2^5, where f_s is the input's sampling frequency.

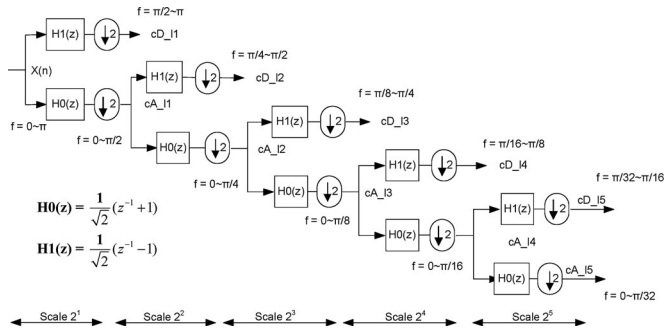

Fig. 4. Cascade filter-bank implementation of DWT.

respectively. The multiscale DWT decomposition is implemented as a cascade filter-bank structure (known as Mallat's Algorithm) illustrated in Fig. 4 featuring high- and low-pass filters. Downsampling is performed after filtering, to remove redundancy. The output of the high-pass filters (H1(z)) provides the detailed WT coefficients (cD_lx) at the 2^x scale, while the approximate WT coefficients (cA_lx) are obtained from the output of the low-pass filters (H0(z)). The frequency resolution increases in higher resolution scales, thus low-frequency components are more easily detectable in high-resolution scales (2^4, 2^5). On the other hand, high-frequency components are expected to be more distinguishable in the lower scales (2^1, 2^2).

From the Haar transfer functions, it can be seen that the output of the high-pass filter is proportional to the local averages of the derivative of the input, which in turn is a filtered version of the original signal. From this, it is established that potential extrema in the original signal x[n] are represented as zero-crossing points in the cD_lx (where x is odd), while instances with maximum slope (deflection points) in the signal are transformed into extrema (minima or maxima) points on the cD_lx. The resolution scales (2^3, 2^5) that we have chosen to operate on, satisfy the aforementioned rule.

Once wavelet coefficients are computed, the focus turns on the 2^3 scale detailed coefficients, where MMA is employed for the approximation of the zero-crossing points. Based on the MMA principle, the boundaries of the constituent ECG waves (P, QRS, and T) are expected, due to their morphology (deflection points), to be localized by a modulus-maxima pair (MMP) on the DWT coefficients of the respective scale.

Given the positive or negative deflection of the ECG wave, compared to the isoelectric line, the pair of extrema that indicates the wave's temporal position, can be either a minimum followed by a maximum, for a positive deflection, or the reverse for a negative deflection. Thus, the MMA method also allows the characterization of every wave as inverted or not, which is exploited in our algorithm, as illustrated in Fig. 5.

Through MMA, we initially obtain the temporal position of the deflection which demonstrates higher separation from the isoelectric line. This is accomplished by calculating the temporal positions (t_1, t_2) of the global extrema pair in the cD_l3 coefficients. This deflection may correspond to either the R_peak (for a positive deflection) or to Q or S_peak (in case of a negative deflection). Next, MMA is applied in the vicinity of the global extrema pair, in order to obtain a first approximation of the temporal position of the QRS boundaries. The initial estimation of the QRS onset ($\hat{\text{QRS}}_{\text{on}}$) is obtained as the preceding

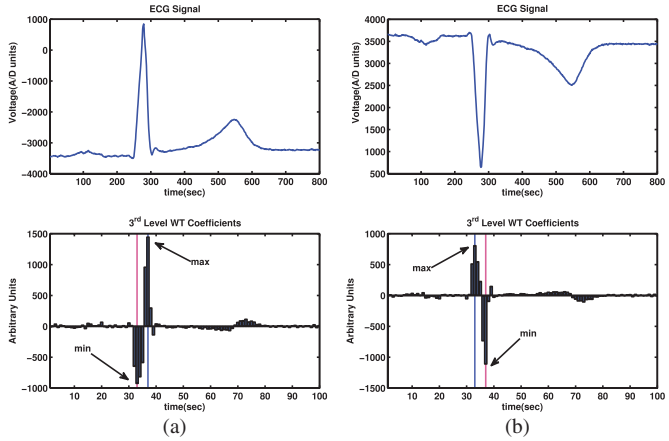

Fig. 5. Characterizing the direction of the deflection based on the sequence of the WT coefficients extrema pair. (a) Positive deflection. (b) Negative deflection.

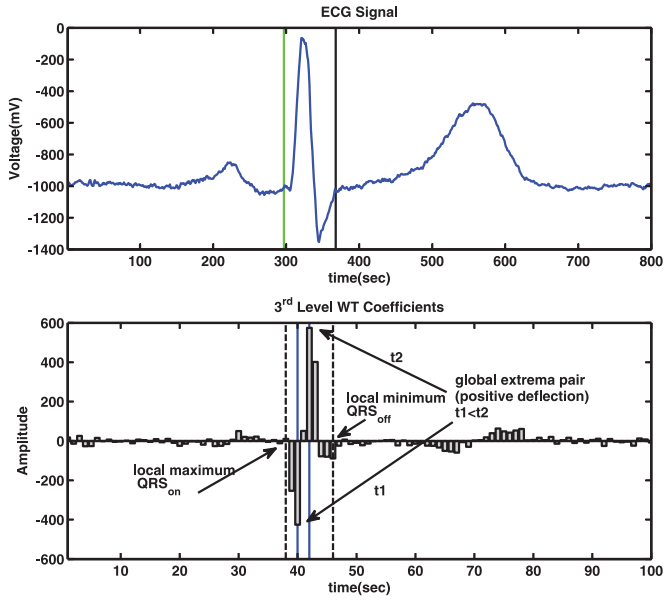

Fig. 6. MMA for the extraction of the QRS boundaries. The global extrema pair localizes the main deflection while the extrema in its vicinity indicate the temporal location of the QRS boundaries.

extrema (min or max) from the local MMP in a search window defined as $[t_1-4, t_1]$. Similarly, the offset of the QRS, ($\hat{\text{QRS}}_{\text{on}}$) is estimated from the succeeding extrema of the MMP found in $[t_2, t_2{+}4]$. Fig. 6 illustrates an example where this procedure is followed to identify the QRS boundaries

As pointed out earlier, the temporal resolution on the 2^3 scale is diminished (by a factor of 8) compared to the original timescale. This coupled with fact that we operate on a single resolution scale, may inherently lead to less accurate localization of the main deflection (either R_peak or Q, S_peak) and of the QRS boundaries. An example where the MMA produces less accurate results is depicted in Fig. 7. For mitigating that effect we employ a TDM-based refinement as described in the following section.

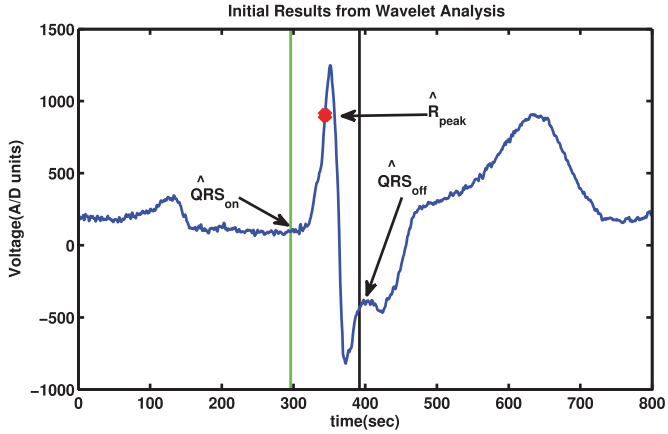

Fig. 7. Example of less accurate estimation of the R_peak and QRS_{off} points due to the decreased temporal resolution of scale 2^3 DWT. These results are ameliorated in TDM stage.

C. TDM-Based Refinement

The TDM refinement process amends the initial MMA approximation, leading to a more accurate estimation of the QRS fiducial points.

The R_peak time instance is amended first. From the MMA on the cD_l3, we obtain the temporal boundaries (t_1, t_2) within which lies the deflection that exhibits higher separation from the isoelectric line. If this deflection is characterized as positive, it is interpreted as an R-wave and thus by projecting (t_1, t_2) into the original timescale of x[n], the amended R_peak time point is calculated as the maximum of the PQRST-complex (max(x[n])) within this time window ($n \in [t_1 \times 2^3,\ t_2 \times 2^3]$). If the deflection detected in the MMA is characterized as negative (t_1 is a maximum and t_2 is a minimum), then it corresponds to either the Q or the S_peak. Since, the R_peak is always a positive deflection, it will be always localized by an MMP with the first point being a minimum and the second a maximum in the cD_l3.

To obtain this pair for this case, we have to consider two possible pairs. We thus search before t_1 for a minimum and after t_2 for a maximum. The search windows are defined as $[t_1 - 15,\ t_1]$ and $[t_2,\ t_2 + 10]$ on the cD_l3 timescale. From this, we obtain two new (t_a-min and t_b-max) local extrema points in cD_l3. From there the two possible pairs of min–max are (t_a, t_1) and (t_2, t_b). Finally, we project the two intervals, $[t_a, t_1]$ and $[t_2, t_b]$, in the x[n] timescale and obtain the maximum value in each one of them. The final R_peak is chosen as the maximum of the two values.

Obtaining the refinement of the R_peak time instance allows us to focus on the refinement of the QRS boundaries. For this, we exploit the characteristic steep slope of the QRS complex by using the derivative signal. The analysis takes place on the approximate 2^3 scale (cA_l3) DWT coefficients. This is chosen from a noise canceling perspective, since we demonstrated that in the 2^3 scale high-frequency noise is removed. The initial QRS boundaries are expanded in time by 64 ms (equivalent of 8 cD_l3 coefficients) before the initial QRS onset ($\acute{t}_3 = t_3 - 8$) and 120 ms (equivalent of 15 cD_l3 coefficients) after the

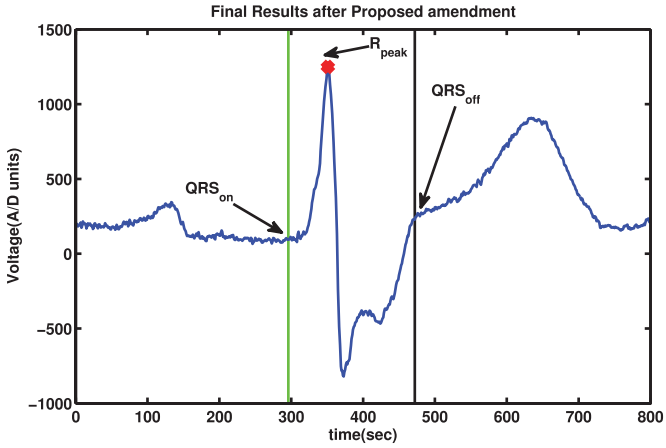

Fig. 8. QRS final estimation on the signal of Fig. 7 after the TDM refinement.

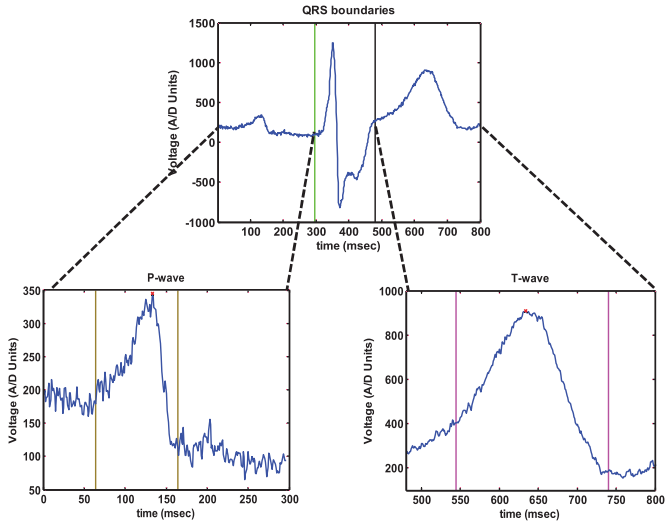

Fig. 9. P and T-wave feature extraction.

initial QRS offset ($\acute{t}_6 = t_6 + 15$). The portion of the ECG signal within these two boundaries is isolated both in x[n] and in cA_l3[n]. This is performed to ensure that the full QRS-complex is contained in the part of the signal we extract in order to apply the refinement. An approximation of the derivative $\acute{f}[n]$ is obtained as the backward difference between two successive samples on the 2^3 scale approximate coefficients cA_l3. We only calculate $\acute{f}[n]$ for $n \in [\acute{t}_3, \acute{t}_6]$.

To identify the QRS boundaries, the derivative signal is investigated against a predefined threshold and the first time point where the value of the gradient signal becomes higher than the predefined threshold corresponds to the amended QRS boundary. For the $\mathrm{QRS_{on}}$ the derivative signal is investigated from the beginning up to the amended R_peak time point ($[\acute{t}_3 \rightarrow \text{R\_peak}]$) while for the $\mathrm{QRS_{off}}$, the gradient signal is investigated from its end toward the R_peak ($[\text{R\_peak} \leftarrow \acute{t}_6]$). The two thresholds for this operation are defined adaptively and their value is set as a dyadic fraction of the amplitude range of the sampled ECG signal. An example where the TDM amends the MMA results is depicted in Fig. 8. In this case, the initial approximation (see Fig. 7) produced by the DWT analysis is improved after the execution of the TDM stage.

The final step of the QRS refinement includes the approximation of the Q_peak and S_peak time instances. The value for these parameters is extracted as the time instance where the ECG signal, in the original timescale, demonstrates minimum value between the QRS-onset and the R_peak and the R_peak and the QRS-offset for the Q_peak and S_peak, respectively. The final outcomes of the amendment process are used in the ultimate stage of the HFEA algorithm which involves the extraction of the clinically relevant features from the P and T-waves.

D. P and T-Wave Feature Extraction

Once the QRS boundaries are finalized after the TDM refinement process, the same modulus-maxima analysis which was applied at the cD_l3 is applied at the 2^5 resolution scale detailed coefficients (cD_l5) only at the portion of the signal that precedes and succeeds the detected QRS complex in order to identify the P and T wave boundaries and the corresponding peaks. These waves are known to demonstrate either convexity or concavity against the isoelectric line and the MMP that localizes the wave, also allows us to characterized it as convex or concave in a similar way that we characterize a deflection as positive or negative. From that point on, the peak of the wave is either the maximum/concave or the minimum/convex point of the original signal x[n] within the modulus-maxima defined wave boundaries. Fig. 9 illustrates the extraction of the fiducial points from the P and T waves, in the PQRST-complex of Fig. 7. The complete HFEA algorithm is given in the form of pseudocode in Fig. 10. The implementation of the algorithm for validation took place in MATLAB.

IV. Computational Complexity and Implementability

To quantify the complexity of the HFEA algorithm, we present here an analytical calculation of the number of arithmetic operations required for the HFEA to run to completion. In principle, there are three major components in the HFEA: the DWT coefficients generation, the MMA and the TDM refinement. Following the flow of the pseudocode in Fig. 10, the upper bound of the number of arithmetic operations is derived considering an input of N samples. In our analysis subtractions are considered equivalent to additions, while one comparison operation is considered to have half the complexity of an addition. Comparisons are used in the extraction of extremas (min/max) within a specific interval. For the sake of complexity analysis, we consider a completely unfolded architecture with no resource sharing and no optimization, like constant number multiplicatoin, for the operations.

To derive the number of arithmetic operations required for the DWT coefficients generation, we consider that for a single cD_lx or cA_lx coefficient, 1 addition, and 1 multiplication is required, according to the Haar DWT high- and low-pass filter transfer functions. In addition, the subsamplers cause each filter output to have half the length of the input. As an example, in order to calculate the cD_l1 or cA_l1 coefficients individually,

1: **Initialise**
2: Consider a PQRST complex x[n] of length l
3: **HAAR DWT**
4: - Calculate DWT Approximate cA_l3 and Detailed Coefficients cD_l3 and Detailed Coefficients cD_l5
5: **QRS Initial Estimation**
6: **Scale 2^3 MMA**
7: Find t_1=min(cD_l3[n])
8: Find t_2=max(cD_l3[n])
9: Find positions (t_3,t_4) of the MMP in cD_l3[n] for $n \in [t_1 - 4, t_1]$ and (t_5,t_6) for $n \in [t_2, t_2 + 4]$
10: Find initial $Q\hat{R}S_{on} = t_3 \times 2^3$
11: Find initial $Q\hat{R}S_{off} = t_6 \times 2^3$
12: **Time-Domain Refinement (TDM)**
13: **if** $t_1 < t_2$ **then**
14: R_peak = max(x[n]), for $n \in (t_1 \times 2^3, t_2 \times 2^3)$
15: **else**
16: Find t_a = min(cD_l3), for cD_l3 $\in [t_1\text{-}15, t_1]$
17: Find t_b = max(cD_l3), for cD_l3 $\in [t_2, t_2\text{+}10]$
18: R_peak1 = max(x[n]), $n \in [t_a \times 2^3, t_1 \times 2^3]$
19: R_peak2 = max(x[n]), $n \in [t_2 \times 2^3, t_b \times 2^3]$
20: Final R_peak = max(R_peak1,R_peak2)
21: **end if**
22: Set $thr1$
23: Set $thr2$
24: Expand $\acute{t}_3 = t_3 - 8$
25: Expand $\acute{t}_6 = t_6 + 15$
26: Approximate Derivative as: $\acute{f}[n] = cA\_l3[n] - cA\_l3[n-1]$, $n \in [\acute{t}_3\ \acute{t}_6]$
27: Final QRS_{on} first $n \in [\acute{t}_3$ R_peak], $f[n] > thr1$
28: Final QRS_{off} last $n \in$ [R_peak $\acute{t}_6$], $f[n] > thr2$
29: Find Q_peak = min(x[n]), $n \in [QRS_{on} \times 2^3$ R_peak]
30: Find S_peak = min(x[n]), $n \in$ [R_peak $QRS_{off} \times 2^3$]
31: **P,T Wave Estimation**
32: **Scale 2^5 MMA**
33: Find t_7 = min(cD_l5[n]), $n \in [1, QRS_{on}]$ for P
34: Find t_8 = max(cD_l5[n]), $n \in [1, QRS_{on}]$ for P
35: **if** $t_7 < t_8$ **then**
36: Calculate $P_{on} = t_7 \times 2^5$
37: Calculate $P_{off} = t_8 \times 2^5$
38: P_peak = max(x[n]) $n \in [\mathrm{P_{on}}\ \mathrm{P_{off}}]$
39: **else**
40: Calculate $P_{on} = t_8 \times 2^5$
41: Calculate $P_{off} = t_7 \times 2^5$
42: P_peak = min(x[n]) $n \in [\mathrm{P_{on}}\ \mathrm{P_{off}}]$
43: **end if**
44: REPEAT P Block with $n \in [QRS_{off}$ cD_l5_end] for the T-wave

Fig. 10. Pseudocode of the HFEA Algorithm.

$N/2$ additions and $N/2$ multiplications are required. Subsequently, the calculation of cD_l2 or cA_l2 requires $N/4$ additions and $N/4$ multiplications. In the HFEA, we only utilize the cD_l3, cA_l3 and cD_l5 coefficients, which according to Mallat's algorithm, means that from the other resolution scales only cA_l1, cA_l2 and cA_l4 must be calculated. In addition, the cA_l5 coefficients do not need to be calculated since cD_l5 are computed directly from cA_l4. In total, the computational complexity of calculating the coefficients that are employed in the HFEA is $N/2 + N/4 + 2N/8 + N/16 + N/32$ additions and $N/2 + N/4 + 2N/8 + N/16 + N/32$ multiplications, or $1.093N$ additions and $1.093N$ multiplications. The MMA step involves the extraction of the max and min values of cD_l3, which is of $N/8$ length. This process requires $(N/8 - 1)$ comparisons. The additional MMA calculations in the vicinity of the global MMA pair require 2 additions for the expansion of t_1, t_2, 4 comparisons in the $[t_1 - 4, t_1]$ interval and another 4 comparisons in the $[t_2, t_2 + 4]$ interval (line 9 of Fig. 10), thus in total 6 additions. At this point the TDM refinement step takes place. The t_1, t_2 values, obtained from MMA (line 7, 8 of Fig. 10) define an interval of length T in the cD_l3 subspace. For the R_peak extraction, the first possibility where $t1 < t2$, (positive major deflection, line 13 of Fig. 10) involves the projection of the T interval boundaries to the original timescale with 2 multiplications, where an interval of length $8 * T$ is now defined and for the extraction of the R_peak $(8T - 1)$ comparisons are required to localize the maximum point and designate it as the R_peak (line 14 of Fig. 10). The second scenario where $t2 < t1$ (negative major deflection, line 15 of Fig. 10 requires 2 additions for the expansion of t_1, t_2 values by 15 and 10, respectively, $((15 - 1) + (10 - 1) = 23)$ comparisons for deriving the t_a and t_b values (lines 16,17 of Fig. 10), 4 multiplications for projecting the t_1, t_2, t_a, t_b into the original timescale and a total of $(8 * 15 - 1) + (8 * 10 - 1) + 1 = 199$ comparisons for the localization and comparison of the R_peak1 and R_peak2 values (lines 18, 19, 20 of Fig. 10). The final R_peak is mapped back to 2^3 scale subspace, with 1 multiplication, where it is used for the QRS boundaries refinement beginning with setting the adaptive thresholds, for which $(N + 2)$ comparisons, 1 addition and 1 multiplication are required. Assuming that the interval of $[t_3, t_6]$ has a length of M, after the expansion by 23 samples in total (2 additions, lines 24, 25 of Fig. 10), the refinement will take place on a sample of $M + 23$ cA_l3 coefficients. For the backward difference operation (gradient calculation) in that sample, $(M + 22)$ additions are required. The operation of comparing the gradient to the thresholds requires, $M + 20$ comparisons for identifying both $\mathrm{QRS_{on}}$ and $\mathrm{QRS_{off}}$. After projecting the QRS boundaries to the original timescale with 2 multiplications, the final stage of the TDM which pertains to the extraction of the Q and S_peak position which requires, $8(M + 23) - (\epsilon_1 + \epsilon_2)$ comparisons, where ϵ_1, ϵ_2 are the differences in samples in the original timescale between the beginning of the $8(M + 23)$ interval and the detected $\mathrm{QRS_{on}}$ and $\mathrm{QRS_{off}}$ and the end of the $8(M + 23)$ interval respectively (lines 29, 30 of Fig. 10).

From the above, the TDM stage collectively requires $11M + N + 203\text{-}1/2(\epsilon_1 + \epsilon_2)$ comparisons, $M + 24$ additions and 6 multiplications, for the first if-statement of the TDM and by following the same process $9M + N + 426 - 1/2(\epsilon_1 + \epsilon_2)$ comparisons, $M + 26$ additions and 8 multiplications for the else-statement. To sum up the calculation of the TDM stage, we consider that $M < N/8, T < M/4$ thus $T < N/32$. Moreover, from our experiments $\epsilon_1, \epsilon_2 < 30$. With these in mind and by expressing comparisons as half additions the total computational complexity of the TDM stage is $1.31N + 95$ additions, 6 mults, or $1.18N + 208$ additions, eight multiplications depending on which if-statement is satisfied.

The final stage of the HFEA for the extraction of the P and T-wave fiducial points initially requires the MMA analysis on the cD_l5 coefficients. For the P-wave, the MMA can theoretically run on a maximum of $N/64$ coefficients and may require upto $(N/64 - 1)$ comparisons to extract the max and min points (lines 33, 34 Fig. 10). Localizing, through MMA, the min and max point of cD_l5 defines an interval of length P which after

being projected (with 2 multiplications, lines 36, 37 Fig. 10) in the original timescale has a length of $8P$. In this interval the P_peak time instance is localized, as the min or max value of the interval and for this $(8P - 1)$ comparisons are used (line 38 Fig. 10). From our experiments $P < N/80$, thus the equivalent number of additions for the P-wave analysis is $0.0391N - 1$ additions and 2 multiplications. For the T-wave analysis, the same number of operations is considered to be required, thus the total number for this stage is $0.0875N - 2$ additions and 4 multiplications. From the above investigation, the total number of operations required for the HFEA algorithm is $2.553N + 102$ additions and $1.093N + 10$ multiplications, or $2.423N + 214$ additions and $1.093N + 12$ multiplications based on which if-statement is executed on the R_peak extraction. This final number represents an upper bound on the required arithmetic operations. It is obvious that the upper bound depends on the number of input samples N. By considering the number of multiplications to be approximately the same for both cases, we focus on the number of additions and conclude that for $N \leq 861$ the upper bound is $2.423N + 214$, while for $N > 861$ the upper bound is $2.553N + 102$. In reality, the number of actual arithmetic operations is going to be lower since $M \ll N/8$, $T \ll N/32$ and the MMA on cD_l5 will be executed on a smaller than $N/64$ number of coefficients.

We now perform a similar analysis on the computational complexity of the WT-delineator in [34]. In this work, which creates the basis of WT-based ECG delineation, the quadratic-spline wavelet is used, with the *algorithme 'a trous* implementation to avoid decimations. From the transfer functions provided, we observe that for computing a single pair of WT coefficients 4 additions and 4 multiplications are required. Since, the number of generated WT coefficients in each level is the same as the number of input samples, for an input of N samples $4N$ additions and $4N$ multiplications are required to generate the WT coefficients in one level. Since the first five scales of WT coefficients are considered $17N$ additions and $17N$ multiplications are needed for the DWT coefficients generation, if the approximate coefficients of the 2^5 are not computed. It is obvious that the amount of required arithmetic operations only for the calculation of the WT coefficients in [34], without any further processing, is considerably higher that the upper bound of the computational complexity of the HFEA. This is indicative of the possibility for significant power reduction, compared to the WT-delineator of [34], of the HFEA when implemented.

In an attempt to estimate how much energy and silicon area the proposed algorithm may consume, we have coded the HFEA in Verilog and synthesized it using the STMicroelectronics 130-nm technology library, following the pseudocode of Fig. 10 without any further architectural optimization. 1-kHz clock frequency and 1.08-V supply voltage were used in our synthesis. The synthesized design has an overall cell area of 245 mm^2, which is equivalent to 404.7 K NAND, and consumes 269.64 nW as calculated from Synopsis PrimeTime tool. The number of clock cycles required for the feature extraction operation on a single PQRST complex constituting of 800 samples is approximately 990 clock cycles.

V. Validation

A. ECG Databases

In order to assess the performance of the proposed algorithm and quantify its accuracy, manually annotated ECG signals from various databases are used. Specifically, 27 ECG excerpts from the QT database (QTDB), 450 from the PTB database (PTBDB), both available at Physionet [6] as well as 144 samples from the Southampton General Hospital Cardiology (SGHCD) department database were used in our validation.

The QTDB contains 105 two-lead Holter ECG recordings sampled at 250 Hz of 15 min duration, covering a wide range of heart conditions. For each sample, the boundaries of the ECG waves (P, QRS, T) and the peaks (P, R, T) temporal position are manually annotated by at least one expert and for at least 30 PQRST complexes in each record, resulting in a total of 3622 annotated complexes [36]. The PTBDB contains 549 high resolution (1 KHz) standard 15-lead ECG recordings, with all leads recorded simultaneously from 294 subjects of several different heart conditions (myocardial infarction, hypertrophy, valvular heart diseases, etc.) as well as sinus rhythm. From SGHCD 12 standard 12-lead paper ECG, sampled at frequencies of 250 and 500 Hz from patients confirmed to be exhibiting myocardial scar were digitized at a rate of 1000 samples/s with the use of the ECGScan digitization software [37] and used in our validation.

From the QTDB, we chose 27 records and applied the HFEA algorithm on every beat on both ECG channels. We specifically selected those records having annotations for every ECG wave (P,QRS, and T). The available manual annotations allowed us to partition the signals into individual ECG heartbeats (by considering the $\mathrm{P_{on}}$ and $\mathrm{T_{off}}$) and then execute the feature extraction algorithm in every one of them. We then calculated the accuracy, in terms of the mean and standard deviation of the error between the algorithm's results and the annotations for each channel separately. Following the guidelines applied in [34], from the two available channels, we finally considered the channel that exhibited less error. The overall mean and standard deviation values are calculated as the average mean and standard deviation of the error from the 27 records.

Different to the QTDB, signals from PTBDB and SGHCD were not preannotated. From the PTBDB, 30 records were chosen from every available disease category. The 30 ECG records of PTBDB and the 12 records of SGHCD resulted in a total of 450 and 144 heartbeats to be given for annotation, respectively. The manual annotations were performed by experts cardiologists with the help of a simple graphical annotator interface also implemented in MATLAB. Whenever the annotation of a particular wave was not possible, either due to the absence of the wave or due to poor sampling, the algorithm's results were disregarded. In order to extract one global temporal position for each fiducial point from the 15 available annotations per record in PTBDB, we followed the k-nearest neighbors (knn) rule applied in [34] for multilead delineators. The 15 onset/offset annotations were ordered in succession and the first time instance which had "k" neighbors within an e ms interval was chosen as

TABLE I
FEATURE EXTRACTION PERFORMANCE RESULTS FROM QTDB

Algorithm	Feature	P_{on}	P_{peak}	P_{off}	QRS_{on}	R_{peak}	QRS_{off}	T_{on}	T_{peak}	T_{off}
HFEA	# ann. beats	1620	1620	1620	1620	1620	1620	1620	1620	1620
	$\mu \pm \sigma$ (ms)	-6.3 ± 12.5	5 ± 9.5	3.1 ± 16	3.7 ± 7.8	3.8 ± 9.8	12.1 ± 16.6	-15.8 ± 34	-15.3 ± 29.3	-16.6 ± 20.8
	σ (samples)	3	2	4	2	2	4	8	7	5
Martinez *et.al.* [34]	# ann. beats	3194	3194	3194	3623	-	3623	-	3542	3542
	$\mu \pm \sigma$ (ms)	2.0±14.8	3.6±13.2	1.9±12.8	4.6±7.7	N/A	0.8±8.7	N/A	0.2±13.9	-1.6±18.1
LPD [38]	# ann. beats	3194	3194	3194	3623	-	3623	-	3542	3542
	$\mu \pm \sigma$ (ms)	14±13.3	4.8±10.6	-0.1±12.3	-3.6±8.6	N/A	-1.1±8.3	N/A	-7.2±14.3	13.5±27.0
CSE [5]	$2\sigma(ms)$	10.2	-	12.7	6.5	-	11.6	-	-	30.6
diff of σ	(samples)	1	-	1	0	-	1	-	4	1

TABLE II
FEATURE EXTRACTION PERFORMANCE RESULTS FROM PTBDB AND SGHCD

Database	Feature	P_{on}	P_{off}	QRS_{on}	QRS_{off}	T_{off}
PTBDB	# ann. beats	422	422	450	450	432
	$\mu \pm \sigma$ (ms)	1.1 ± 9.5	-6 ± 11	3.8 ± 10.8	3.7 ± 6.8	-8 ± 10.8
SGHCD	# ann. beats	128	128	144	144	132
	$\mu \pm \sigma$ (ms)	8.8 ± 14.4	-1.8 ± 15.7	4.1 ± 16.2	6 ± 14.3	-3.8 ± 21.3
CSE [5]	2σ	10.2	12.7	6.5	11.6	30.6

the wave onset. Conversely, the last time instance obeying in the same knn rule is characterized as the wave offset. We also employed the same multilead rule in the results obtained from our algorithm. For these signals, since only one heartbeat per lead is annotated the mean and the standard deviation were calculated from the error between the annotations and the algorithm's results for the 30 records.

In the SGHCD ECG samples, the 12 leads were captured simultaneously in groups of 3 leads. As a result the previous *knn* rule could not be applied. For these signals, we followed the CSE guidelines as described in [12]. In every record, the 12 leads were divided into four groups each containing the three simultaneously captured leads. The groups were formed of leads I–III, aVR–aVF, V_1–V_3, V_4–V_6. For each leadgroup, the earliest onset and the latest offset were selected as the global temporal positions of the boundaries of ECG waves. Based on this rule, we then calculated the mean and standard deviation between the HFEA results and the manual annotations for each leadgroup separately using all 12 records. The final results were produced by averaging the mean and standard deviation of the four leadgroups.

B. Results and Discussion

Table I lists accuracy results in terms of mean μ and standard deviation σ attained from executing the HFEA on 27 records from the QTDB. Apart from the mean μ and the standard deviation σ in ms, we provide the standard deviation in the equivalent number of samples rounded toward the nearest integer. We also list the performance of the quadratic-spline-based WT delineator, presented in [34] as well as results of the low-pass-differentiator (LPD) method reported in [38], from the same database. The final row lists the tolerance limits for automatic feature extraction algorithms as were defined by the CSE Working party in [5]. Although in the QTDB results the HFEA algorithm satisfies the CSE tolerance limitonly for the T-wave offset, the interpretation of the CSE limits in the QTDB, as also expressed in [34], can not be straightforward due to the limited number of different annotators in the QTDB. Compared to the quadratic-spline WT delineator and the LPD the HFEA demonstrates comparable results, since only the QRS offset and T-wave peak position are estimated with considerable less accuracy. In the final row, we provide the difference of the standard deviations between the HFEA and the CSE tolerance limits in terms of the number of samples, based on the sampling frequency of the database (i.e., 1 sample $=$ 4 ms). Wherever there is no CSE tolerance we used the lowest standard deviation among the WT delineator by Martinez *et al*. and LPD. This result was not produced for the P_peak where the HFEA demonstrated the best performance of the three algorithms and there are no CSE tolerance limits. It is to be noted that for these parameters that the CSE limit is not satisfied, the error, in terms of the actual ECG samples, is one sample, except from T_peak.

Table II lists performance results obtained from the 450 signals of PTBDB and the 144 signals of SGHCD. Both databases facilitated the assessment of the HFEA performance in a multilead ECG system. The knn and the earliest(onset)-latest (offset) rules, described in Section V-A, were used to obtain the global temporal position of each parameter for each record from the 15 simultaneously recorded leads of PTBDB and for each leadgroup in SGHCD. In this investigation, we restricted ourselves to the parameters for which CSE tolerance limits are provided and the mutlilead knn rule has been applied previously [34], [39].

Although a different database, PTBDB allows for a more valid comparison with the CSE tolerance limits since it also contains standard 15-lead recordings. The best performance was observed for $k = 3$ neighbors for all parameters, and $e = 10$ ms for the P-wave boundaries and $\mathrm{QRS_{on}}$ while $e = 12$ ms was used for the $\mathrm{QRS_{off}}$ and the $\mathrm{T_{off}}$. From the results, we observe that all CSE tolerance limits are satisfied apart from the one for $\mathrm{QRS_{on}}$.

The obtained results from the digitized SGHCD database are also given in Table II. This paper digitization process diminished the quality of the actual recordings, thus only one CSE limit $\mathrm{T_{off}}$ was satisfied in these signals. In spite of this, the outcome of the HFEA algorithm was endorsed by cardiologists.

VI. Conclusion

In this paper, a novel algorithm (HFEA), based on the combination of WT analysis and time-domain morphology principles, for extracting the ECG fiducial points is proposed. The HFEA is tailored for application in energy constrained remote CVD monitoring environments. The use of DWT with the Haar function as the basis allows for a significant reduction in the computational complexity compared to other WT-based approaches, which is beneficial in terms of the overall energy consumption. Experiments carried out on ECG signals from publicly available databases, covering both standard 12-lead (PTBDB) and ambulatory (QTDB) recordings, as well as on a noncommercial database (SGHCD) show that the HFEA performance is very close to the state-of-the-art ECG delineators. When comparing the HFEA results from PTBDB to the CSE tolerance limits, all but one ($\mathrm{QRS}_{\mathrm{on}}$) are satisfied. Although slightly less accurate, the computational complexity, in terms of the required mathematical operations of our approach, which is found to be $2.423N + 214$ additions and $1.093N + 12$ multiplications for $N \leq 861$ or $2.553N + 102$ additions and $1.093N + 10$ multiplications for $N > 861$, is significantly smaller than that of the other WT-based approaches. This facilitates the implementation of the HFEA in ultralow-power systems, in the form of a standalone ASIC, enabling the long-term deployment of the HFEA architecture in battery power devices. By taking into account that mobile CVD monitoring systems are predominantly used for assessing the patient's overall condition, rather than making a complete diagnosis, the proposed scheme is an ideal candidate for the ECG analysis in such systems.

References

[1] Frost & Sullivan. (2009). "Preparing for an aging society: Challengers faced by healthcare system in European Union, Japan and United States," [Online]. Available: http://www.frost.com/

[2] R. Balani, "Energy consumption analysis for bluetooth, WiFi and cellular networks," Univ. California at Los Angeles, Tech. Rep. TR-UCLA-NESL-200712-01, 2007

[3] Chiron Project. (2010). [Online]. Available: www.chiron-project.eu

[4] F. Rincón, J. Recas, N. Khaled, and D. Atienza, "Development and evaluation of multilead wavelet-based ECG delineation algorithms for embedded wireless sensor nodes," *IEEE Trans. Inf. Technol. Biomed.*, vol. 15, no. 6, pp. 854–863, Nov. 2011.

[5] "The CSE working party, "Recommendations for measurement standards in quantitative electrocardiography," *Eur. Heart J.*, vol. 6, no. 10, pp. 815–825, Oct. 1985.

[6] A. L. Goldberger *et al.*, "Physiobank, physiotoolkit, and physionet components of a new research resource for complex physiologic signals," *Circulation*, vol. 101, no. 23, Jun. 13, 2000.

[7] M. Nygårds and L. Sörnmo, "Delineation of the QRS complex using the envelope of the E.C.G.," *Med. Biol. Eng. Comput.*, vol. 21, pp. 538–547, 1983.

[8] O. Pahlm and L. Sörnmo, "Software QRS detection in ambulatory monitoring a review," *Med. Biol. Eng. Comput.*, vol. 22, pp. 289–297, 1984.

[9] J. Pan and W. J. Tompkins, "A real-time QRS detection algorithm," *IEEE Trans. Biomed. Eng.*, vol. 32, no. 3, pp. 230–236, Mar. 1985.

[10] P. S. Hamilton and W. J. Tompkins, "Quantitative investigation of QRS detection rules using the MIT/BIH arrhythmia database," *IEEE Trans. Biomed. Eng.*, vol. 33, no. 12, pp. 1157–1165, Dec. 1986.

[11] L. Sörnmo, "A model-based approach to QRS delineation," *Comput. Biomed. Res.*, vol. 20, pp. 526–542, Dec. 1987.

[12] J. Willems *et al.*, "Assessment of the performance of electrocardiographic computer programs with the use of a reference data base," *Circulation*, vol. 71, no. 3, pp. 523–525, Mar. 1985

[13] F. Gritzali, "Towards a generalized scheme for QRS detection in ECG waveforms," *Signal Process.*, vol. 15, pp. 183–192, Sep. 1988.

[14] Z. Dokur, T. Olmez, M. Korurek, and E. Yazgan, "Detection of ECG waveforms by using artificial neural networks," in *Proc. IEEE Eng. Med. Biol. Soc.*, Oct.-3 Nov. 1996, vol. 3, pp. 929–930.

[15] E. Soria-Olivas, et al., "Application of adaptive signal processing for determining the limits of P and T waves in an ECG," *IEEE Trans. Biomed. Eng.*, vol. 45, no. 8, pp. 1077–1080, Aug. 1998.

[16] R. V. Andreão, B. Dorizzi, and J. Boudy, "ECG signal analysis through Hidden Markov Models," *IEEE Trans. Biomed. Eng.*, vol. 53, no. 8, pp. 1541–1549, Aug. 2006.

[17] Z. Yong, H. Wenxue, X. Yonghong, and C. Jianxin, "ECG beats classification based on ensemble feature composed of independent components and QRS complex width," in *Proc. Int. Conf. Comput. Sci. Softw. Eng.*, Dec. 2008, vol. 1, pp. 868–871.

[18] M.-Y. Yang, W.-C. Hu, and L.-Y. Shyu, "ECG events detection and classification using wavelet and neural networks," in *Proc. IEEE Eng. Med. Biol. Soc.*, Oct./2 Nov. 1997, vol. 1, pp. 289–292.

[19] Z. Dokur, T. Olmez, and E. Yazgan, "ECG waveform classification using the neural network and wavelet transform," in *Proc. IEEE Eng. Med. Biol. Soc.*, 1999, vol. 1, p. 273.

[20] S. Szilágyi and L. Szilágyi, "Wavelet transform and neural-network based adaptive filtering for QRS detection," in *Proc. IEEE Eng. Med. Biol. Soc.*, Jul. 2000, vol. 1, pp. 1267–1270.

[21] S. Szilagyi, Z. Benyo, L. Szilagyi, and L. David, "Adaptive wavelet-transform-based ECG waveforms detection," in *Proc. IEEE Eng. Med. Biol. Soc.*, Sep. 2003, vol. 3, pp. 2412–2415.

[22] R. V. A. Andreão and J. Boudy, "Combining wavelet transform and hidden Markov models for ECG segmentation," *EURASIP J. Appl. Signal Process.*, vol. 2007, pp. 95–95, Jan. 2007

[23] G. de Lannoy, B. Frenay, M. Verleysen, and J. Delbeke, "Supervised ECG delineation using the wavelet transform and hidden Markov models," in *Proc. Conf. Int. Federation Med. Biol. Eng.*, 2008, vol. 22, pp. 22–25.

[24] C. Li, C. Zheng, and C. Tai, "Detection of ECG characteristic points using wavelet transforms," *IEEE Trans. Biomed. Eng.*, vol. 42, no. 1, pp. 21–28, Jan. 1995.

[25] S. Kadambe, R. Murray, and G. Boudreaux-Bartels, "The dyadic wavelet transform based QRS detector [ECG analysis]," in *Proc. 26th Asilomar Conf. Signals, Syst. Comput.*, Oct. 1992, vol. 1, pp. 130–134.

[26] V. Di Virgilio, C. Francaiancia, S. Lino, and S. Cerutti, "ECG fiducial points detection through wavelet transform," in *Proc. IEEE Eng. Med. Biol. Soc.*, Sep. 1995, vol. 2, pp. 1051–1052.

[27] J. Sahambi, S. Tandon, and R. Bhatt, "Using wavelet transforms for ECG characterization. An on-line digital signal processing system," *IEEE Eng. Med. Biol. Mag.*, vol. 16, no. 1, pp. 77–83, Jan./Feb. 1997.

[28] M. Bahoura, M. Hassani, and M. Hubin, "DSP implementation of wavelet transform for real time ECG wave forms detection and heart rate analysis," *Comput. Methods Progr. Biomed.*, vol. 52, no. 1, pp. 35–44, 1997.

[29] S. Mahmoodabadi, A. Ahmadian, M. Abolhasani, M. Eslami, and J. Bidgoli, "ECG feature extraction based on multiresolution wavelet transform," in *Proc. IEEE Eng. Med. Biol. Soc.*, Jan. 2005, pp. 3902–3905.

[30] K. Ouni, S. Ktata, and N. Ellouze, "Automatic ECG segmentation based on Wavelet Transform Modulus Maxima," in *Proc. IMACS*, Oct. 2006, vol. 1, pp. 140–144.

[31] A. Josko, "Discrete wavelet transform in automatic ECG signal analysis," in *Proc. IEEE Instrum. Meas. Technol. Conf.*, May 2007, pp. 1–3.

[32] Y. Velchev and O. Boumbarov, "Wavelet transform based ECG characteristic points detector," in *Proc. Int. Sci. Conf. Comp. Sci.*, 2008, vol. 1, pp. 22–25.

[33] J. Martinez, S. Olmos, and P. Laguna, "Evaluation of a wavelet-based ECG waveform detector on the QT database," in *Comput. Cardiol.*, 2000, pp. 81–84.

[34] J. Martinez, R. Almeida, S. Olmos, A. Rocha, and P. Laguna, "A wavelet-based ECG delineator: evaluation on standard databases," *IEEE Trans. Biomed. Eng.*, vol. 51, no. 4, pp. 570–581, Apr. 2004.

[35] A. Burns *et al.*, "Shimmer$^{\mathrm{TM}}$—A wireless sensor platform for noninvasive biomedical research," *IEEE Sensors J.*, vol. 10, no. 9, pp. 1527–1534, Sep. 2010.

[36] P. Laguna, R. Mark, A. Goldberg, and G. Moody, "A database for evaluation of algorithms for measurement of QT and other waveform intervals in the ECG," in *Proc. Comput. Cardiol.*, Sep. 1997, pp. 673–676.

[37] F. Badilini, T. Erdem, W. Zareba, and A. Moss, "ECGScan: A method for conversion of paper electrocardiographic printouts to digital

electrocardiographic files," *J. Electrocardiol.*, vol. 38, no. 4, pp. 310–318, Oct. 2005.
[38] P. Laguna, R. Jané, and P. Caminal, "Automatic detection of wave boundaries in multilead ECG signals: Validation with the CSE database," *Comput. Biomed. Res.*, vol. 27, pp. 45–60, Feb. 1994.
[39] P. de Chazal and B. Celler, "Automatic measurement of the QRS onset and offset in individual ECG leads," in *Proc. IEEE Eng. Med. Biol. Soc.*, 1996, vol. 4, pp. 1399–1400.

Evangelos B. Mazomenos received the Diploma degree in electrical and computer engineering from the University of Patras, Patras, Greece, and the Ph.D. degree from the School of Electronics and Computer Science, University of Southampton, Southampton, U.K., in 2006 and 2012, respectively.

Since January 2011, he has been a Research Fellow in the School of Electronics and Computer Science, University of Southampton. His research interests include the area of wireless sensor networks (WSNs) with a focus on positioning and tracking, biomedical signal processing, and dynamic estimation algorithms.

Dr. Mazomenos is the recipient of the 2009 IET Leslie H. Paddle fellowship on post-graduate studies for his Ph.D. research on real-time target tracking in WSN.

Dwaipayan Biswas received the M.Sc. degree in system on chip from the University of Southampton, Southampton, U.K., in 2011, where he is currently working toward the Ph.D. degree in biomedical engineering with the Electronics and Software Systems Group.

His research interests include biomedical signal processing and low power very large scale integration design.

Amit Acharyya received the Ph.D. degree from the School of Electronics and Computer Science, University of Southampton, Southampton, U.K., in 2011.

He is currently an Assistant Professor in the Indian Institute of Technology (IIT), Hyderabad, India. His research interests include signal processing algorithms, very large scale integration architectures, low power design techniques, computer arithmetic, numerical analysis, linear algebra, bioinformatics, and electronic aspects of pervasive computing.

Taihai Chen received the B.Eng. degree (1st Class Hons.) from the University of Electronic Science and Technology of China, Chengdu, China, in 2009, and the M.Sc. degree (Distinction) from the University of Southampton, Southampton, U.K., in 2010, where since October 2010, he has been working toward the Ph.D degree with Electronic and Software Systems Research Group.

His research interests include biomedical signal processing, low-power design techniques, pattern recognition, machine learning, associated very large scale integration architectures, and next-generation healthcare systems.

Koushik Maharatna (M'02) received the M.Sc. degree in electronic science from Calcutta University, Calcutta, India, in 1995, and the Ph.D. degree from Jadavpur University, Calcutta, India, in 2002.

From 1996 to 2000, he was involved in different projects sponsored by the Government of India undertaken at the Indian Institute of Technology (IIT), Kharagpur, India. From 2000 to 2003, he was a Research Scientist in IHP, Frankfurt (Oder), Germany. During this phase, his main involvement was related to the design of a single-chip modem for the IEEE 802.11a standard. In September 2006, he joined the School of Electronics and Computer Science, University of Southampton, Southampton, U.K., where he is currently a Reader. His research interests include low-power very large scale integration (VLSI) and signal processing for applications in DSP, communication and next-generation healthcare systems, computer arithmetic, analog signal processing, and bioinspired circuits and systems.

Dr. Maharatna is a member of the IEEE VLSI System Application Technical Committee.

James Rosengarten received the MBBS degree from the University of London, U.K., in 2002.

Currently, he is a Clinical Cardiologist based in Southampton. Following training in general cardiology in London and Wessex, he is now specializing in heart rhythm disorders, including invasive testing and implantable devices. He is currently the Research Fellow in Cardiac Rhythm Management, based at University Hospital Southampton, Southampton, U.K. Under the supervision of Prof. Morgan and Prof. Hanson at the University of Southampton, he is utilizing engineering techniques to discover novel biomarkers of sudden cardiac death risk.

Dr. Rosengarten became a member of the Royal College of Physicians (MRCP(U.K.)) in 2005.

John Morgan graduated from the University of Cambridge, Cambridge, U.K., with a B.A. in natural sciences in 1979 from the Westminster Medical School, London, U.K. with an MB BChir in 1982, and the M.A. and M.D. degrees from Cambridge University, Cambridge, in 1983 and 1991, respectively.

He is currently with the Southampton University Hospitals NHS Trust, Southampton, U.K. He became a member of the Royal College in 1985 and Fellow in 1995. On his appointment as a Consultant Cardiologist, Wessex Cardiothoracic Centre in 1992, he founded the Wessex Cardiac Arrhythmia Management Service which has become recognized as a Centre of Clinical and Research Excellence. He was appointed an Honorary Professor at the University of Teesside in 2006 for his work in medical education and received the Personal Chair in the School of Medicine, University of Southampton, in 2007. He holds several published patents relating to invention of novel interventional and device technologies. He supervises/has supervised several fellows in doctoral research projects and continues to research and publish extensively and is an internationally recognized leader in his field. He also sits on a series of national and international boards/professional associations and governing bodies.

Nick Curzen was trained in cardiology at Southampton, Bournemouth, Royal Brompton, London Chest and St Bartholomews hospitals, between 1993 and 1996. He received the Ph.D. degree in vascular biology at Imperial College, London, U.K., in 1996.

He is a Consultant Cardiologist at University Southampton Hospitals and a Professor of Interventional Cardiology at the University of Southampton, Southampton, U.K. He has wide ranging research interests including platelet function, myocardial ischaemia, cardiac magnetic resonance, and scar. He has more than 130 peer review scientific papers and has edited three cardiology textbooks. In November 2010, he came top of a national poll of interventional cardiologist published in the Daily Mail.